

# 3rd Year Mini Project - The Helium Neon LASER

Kylie J MacFarquharson

May 11, 2018

## **Abstract**

In this experiment we built a large He-Ne LASER with an open cavity. We then investigated various properties of the LASER by inserting optical components into the cavity. In particular we looked further into single longitudinal mode operation of the LASER by using a frequency selector. In this experiment we showed that the helium-neon mix had a gain coefficient of  $\approx 0.084\text{m}^{-1}$ . We also demonstrated sufficient frequency resolution to pick out the individual LASER peaks at 632.8nm and 611.9nm.

# 1 Introduction

The first LASER was built at Hughes Research Laboratories in 1960, using ruby as a gain medium [2]. The first helium neon LASER was built later in the same year [1]. Since then, LASERS have become commonplace in industry, technology, and research. A number of properties make them more useful than other light sources such as a high intensity, high peak power output, and a fixed phase relationship between all parts of the beam. This makes them very useful for reading data as in CD's, heating of small objects, or experiments involving very high electric fields. As such the benefits of investigating these devices is clear.

The first part of this experiment involved building a helium-neon LASER along an optical rail. The lasing of the device occurs in energy transitions in neon. The helium allows pumping of the higher energy levels by the process shown in Figure 1.1. Constructing a LASER requires very high precision alignment of all devices as well as very high quality optical components as a loss of even 1% can stop lasing from occurring. To achieve this high level of precision we defined the optical axis using a second, low-power He-Ne LASER.

In order to build an appropriate cavity we used mirrors with dielectric coatings to make them highly reflective at the lasing frequency of He-Ne ( 632.8nm). Any dust or oil on these could destroy the LASER so they were stored with firmly attached dust covers. They also had no back, meaning that the tiny amount of light not reflected would be transmitted through and could be used as the output of the LASER.

The mirrors available to us were a plane mirror with reflectivity near 100% (denoted [PLANE]), a plane mirror with reflectivity of 97.6% (denoted [2.4%]), and focusing mirrors with radius 1000mm and 700mm (denoted [R1000] and [R700] respectively).

# 2 Construction

We could then align each of the mirrors by aligning the laser dot with its reflection on each of the mirrors. This worked as the laser output was obviously highly reflective to it's own light. When the beam was correctly aligned we had created a 1D optical cavity with coherent light. As such, a very visible interference pattern is seen upon correct alignment of a mirror, as seen in Figure 2.1. The final component, the He-Ne discharge tube was aligned by projecting the laser onto a diffuse white surface, approximately 2m away, creating a visible spot. The tube was inserted onto the optical rail and it's position and angle adjusted until the projected spot was circularly symmetric, meaning that we tube was on axis. Using two mirrors and the discharge tube, the laser was constructed and activated. Further adjustments to the alignments were made until the device began to lase. Final adjustments brought the laser brightness to a maximum.

The first laser build used mirrors [R700] and [PLANE]. This reduced losses and meant the window for lasing was much broader. For the first experiments we wanted to increase power outputs and so the output coupling laser [PLANE] was switched with [2.4%]. This increased the output from 0.2mW to 5mW but made alignment much harder, as fewer losses were tolerable.

We also constructed a simple Michelson Interferometer as detailed in [3]. This allowed us to investigate some of the phase properties of the LASER.

# 3 Initial Experiments

The first experiment we planned was to measure the output power of the tube as a function of tube current. To measure power output a photodiode was placed in the path of the beam and the power measured (in arbitrary units). The data can be seen in Table C.1. However, as can be seen in Figure 3.1 the curve is not a simple polynomial, meaning the relationship is more complex. A further effect was noticed, runs done later in time had consistently higher power outputs. To see if this was a significant effect we left the LASER running on maximum current (6.5mA) for around 30m. We noticed that the output power had reached 8 arbitrary units. We suspect this is due to increasing temperature of the tube.

# 4 Lasing Frequencies

Figure 1.1 suggests that a number of different lasing frequencies are available. In order to investigate this, we replaced the output coupling mirror with a Littrow prism. When tuned correctly, this functioned as a frequency selector and small rotations of the mirror allowed us to sweep through a large range of wavelengths ( $\sim 5\text{nm}$ ). Due to broadening in the prism,

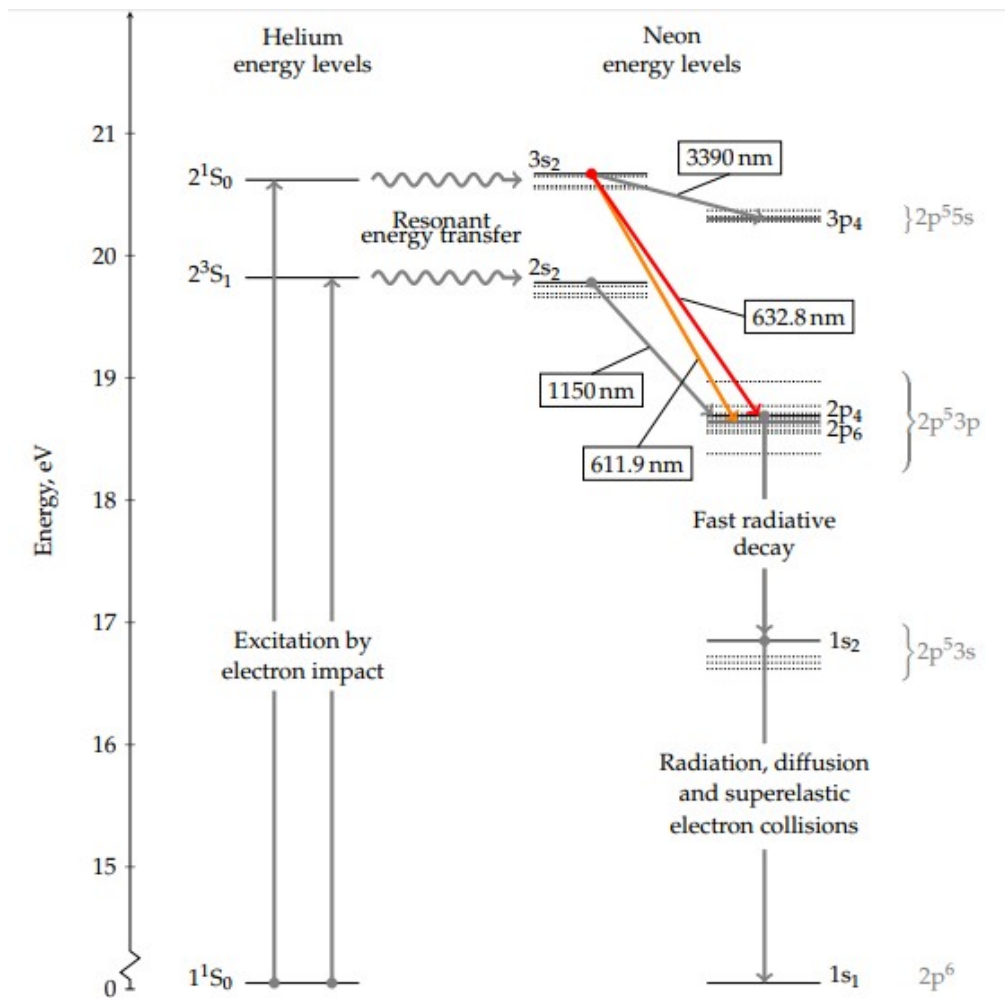


Figure 1.1: Energy levels of helium and neon on the same scale, showing transitions in the helium neon laser for the brightest output wavelengths. Adapted from [7]

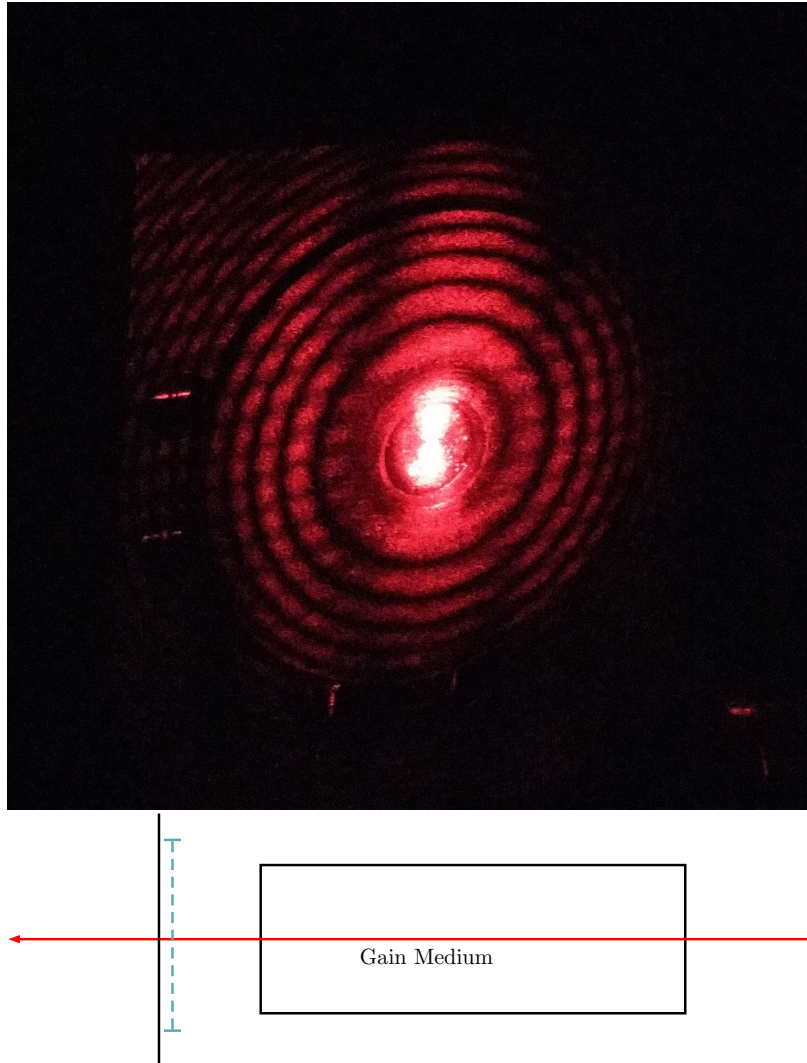


Figure 2.1: Interference fringes on the inside of the cavity caused by correct alignment of mirror. Note that the horizontal lines are due to a rolling shutter effect in the camera. *Schematic diagram shows picture location with dashed line*

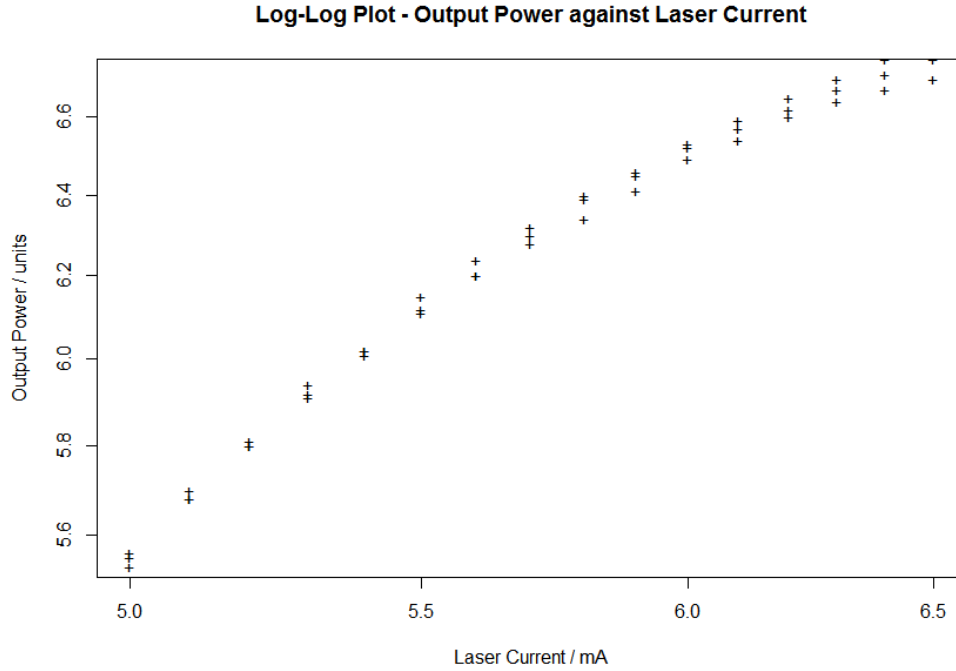


Figure 3.1: Output power of helium-neon LASER measured by photodiode in normalised arbitrary units at 632.8nm plotted against input current into the discharge tube. Tabulated data is available in Table C.1

the selection envelope is fairly wide. However, any peaks in brightness of the LASER can be nothing other than a LASER transition. Three such peaks were observed, all of which looked close to red. We took these to be the 632.8nm, 629.4nm, and 611.9nm transitions in neon [6]. Images of some of these beams can be seen in Figure 4.1.

## 5 Longitudinal Modes

A continuous wave LASER requires a standing wave to be formed in the cavity, meaning only certain frequencies can lase. These frequencies  $\nu_c$  allowed by the cavity length  $L_c$  are given by

$$\nu_c(n) = \frac{cn}{2L_c} \tag{5.1}$$

for any integer  $n$ .

At absolute zero this would make lasing almost impossible as the cavity would have to be constructed with infinite precision. However, the LASER peaks are Doppler broadened, expressed as

$$\frac{\Delta\nu_D}{\nu_D} = 2\sqrt{2\ln(2)}\sqrt{\frac{k_B T}{Mc^2}}. \tag{5.2}$$

Evaluating Equation (5.1) and Equation (5.2) numerically we can find

$$\Delta\nu_c = \frac{c}{2L_c} \approx 312\text{MHz}$$

for  $L_c \approx 0.5\text{m}$ ,

and

$$\Delta\nu_D \approx 2\text{GHz}$$

for  $T \approx 600\text{K}$ .

The Doppler broadening is much larger than the spacing between allowed cavity states. As such the transition that is lasing will be broadened to include several longitudinal modes in the envelope that has sufficient gain for lasing.

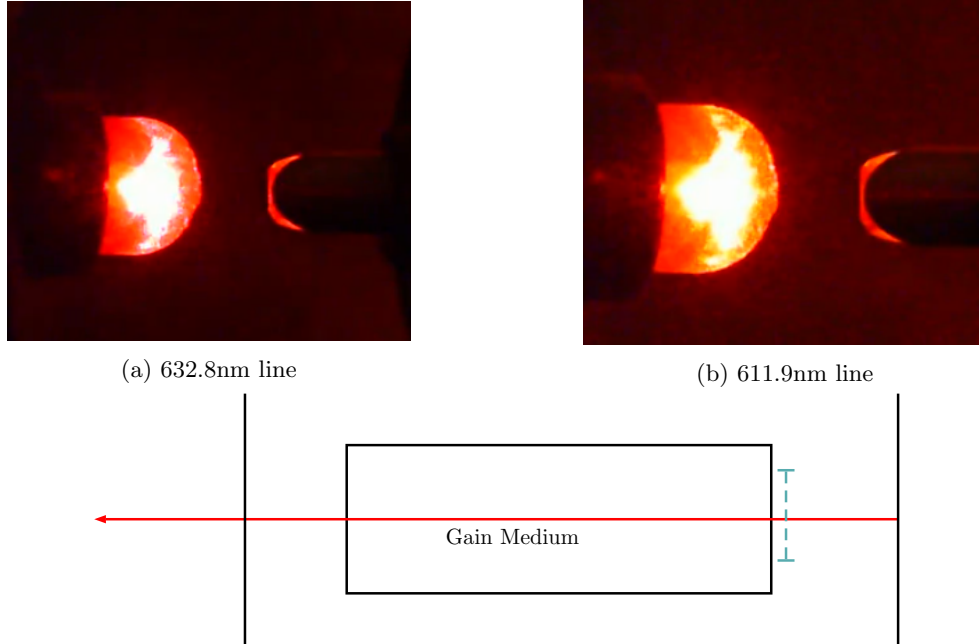


Figure 4.1: Two transitions of the helium-neon LASER in single longitudinal mode operation selected for with a Littrow Prism .  
To be viewed on a colour screen.

## 5.1 Single Longitudinal Mode Operation

Using a frequency selector we can force only one longitudinal mode to form an optical cavity. We call this single longitudinal mode (SLM) operation. We use an etalon to pick out frequencies as a rotation with a micrometer allows us to sweep through frequency space. Whether the etalon is sufficient for SLM operation can be checked with the condition in Appendix B.

Sweeping through frequency space in this way gave us 14 different longitudinal modes that will lase. And so the envelope of frequencies with sufficient gain to lase has width  $\Delta v_{osc}$  given by

$$\Delta v_{osc} \approx 15(1)\Delta v_c ,$$

Which evaluates to

$$\Delta v_{osc} = 4.5(3)\text{GHz} \approx 2\Delta v_D . \quad (5.3)$$

One benefit of SLM Operation is that the very narrow linewidth means that the coherence length is very large compared to that of the standard operation of the LASER. We planned to test this using a Michelson interferometer. To get visible fringes we used an expander to increase the spot size. Both operations of the LASER created clear fringes throughout the length range of the interferometer, an example of the fringes visible in Figure 5.1. We proceeded to search for fringes in each operation at larger distances, finding clear fringes even at distances of  $\sim 50\text{mm}$ . This was unexpected and so we added a sharp object into the path of the beam to give us a clear idea of alignment. The output from the Michelson Interferometer can be seen in Figure 5.2a. However, with this imaging we noticed a fine structure of parallel lines, which we determined to be upstream of the interferometer. We were concerned these would generate a Moiré pattern, indistinguishable from an interference. To test the possibility of this we deliberately misaligned the interferometer and looked for a pattern resembling interference fringes. The result can be seen in Figure 5.2b. It was not possible to identify true interference with our experimental set-up.

## 6 Transverse Modes

Also to consider is the transverse profile of the beam. It is clear the beam does not fill the gain medium but instead has a small Gaussian profile due to the boundary conditions imposed at the focusing mirror. As such, quantised transverse modes describe the allowable beam profiles.

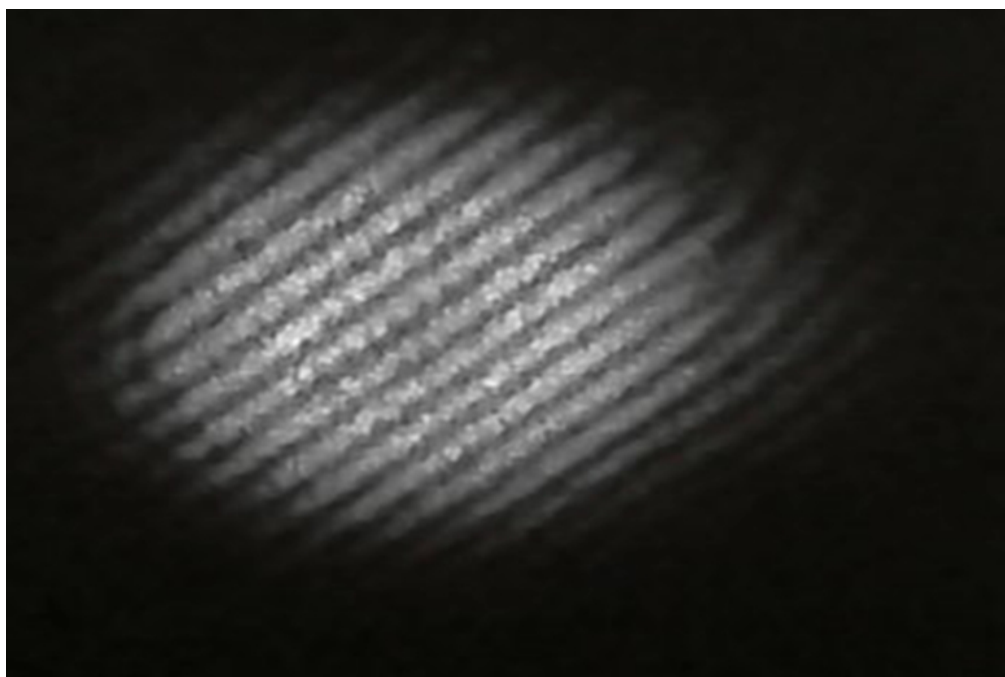
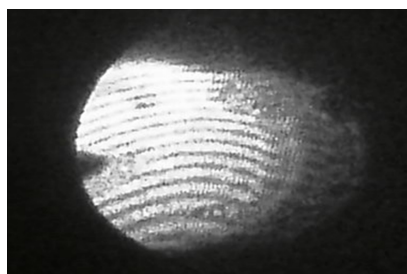
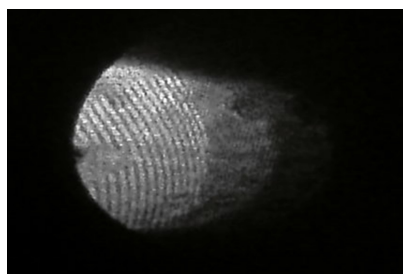


Figure 5.1: Image of interference fringes from a helium-neon LASER at 632.8nm produced by a Michelson interferometer



(a) Image of Interference Fringes



(b) Image of Moiré Fringes

Figure 5.2: Image of two varieties of fringes from a helium-neon LASER source at 632.8nm produced by a Michelson interferometer

The transverse modes of the LASER are given by Gauss-Hermite beams [5, Section 6.3.2]:

$$\begin{aligned}
U = & i \frac{U_0}{z_R} \exp(i(kz - \omega t)) \\
& \times \frac{w(z_0)}{w(z)} \exp(-[r/w(z)]^2) \\
& \times H_l \left[ \sqrt{2} \frac{x}{w(z)} \right] H_m \left[ \sqrt{2} \frac{y}{w(z)} \right] \\
& \times \exp[ikr^2/2R(z)] \\
& \times \exp[-i(l + m + 1)\alpha]
\end{aligned} \tag{6.1}$$

## 6.1 Lowest Order Mode

In the lowest order mode TEM<sub>00</sub>, the beam has a purely Gaussian profile, creating the familiar “spot” image. The FWHM of this is given by  $\sqrt{2 \ln 2} w(z)$  with the “spot radius”  $w(z)$  given by

$$w(z) = w(z_0) \sqrt{1 + \left( \frac{z - z_0}{z_R} \right)^2}, \tag{6.2}$$

with *confocal parameter*:

$$z_R = \frac{\pi w(z_0)^2}{\lambda}, \tag{6.3}$$

a hyperbola with the minimum (*beam waist*) at  $z_0$ .

It can be shown that a maximum value for the cavity length exists, above which lasing is impossible. Simple geometry shows that to prevent scattering,  $L_c < R$  is required if one of the mirrors is a plane mirror. The output power of the LASER with various cavity lengths was measured to test this theory, using the mirrors [PLANE], and [R700]. This data can be seen in Figure 6.1 and it is clear that there is a maximum cavity length near 700mm.

Our next experiment involved measuring the spot width by placing a slit of variable width in the optical cavity. The effect of this is that at a certain critical width  $w_{crit}$ , a sufficient amount of light will be blocked such that the losses exceed the allowable amount and the LASER will cease to function. It shown in Appendix A that this  $w_{crit}(z)$  is proportional to the spot radius  $w(z)$ . In this way, we measure  $w_{s,crit}(z)$  throughout the cavity.

The results are shown on Figure 6.2. Fitting this curve to Equation (6.2) gives us *beam waist position*  $z_0 = 0$ , *critical slit width at beam waist*  $w_{s,crit}(z_0) = 740(?)\mu\text{m}$ , and a *confocal parameter*  $z_R = 340(?)\text{mm}$ .

Equation (6.3) gives us

$$w(z_0) = 262(5)\mu\text{m}$$

and so, from Equation (A.2),

$$w'_{crit} = \frac{w_{crit}(z)}{w} = 2.8(1).$$

And finally, Equation (A.1) gives us the critical transmission of the slit, below which the device will not lase at of  $T = 0.995(2)$ . This effectively gives us our one pass optical gain as  $T^2 g^2 R_1 R_2 = 1$  so  $g = 1.017$ .

This is a significant result as it shows that a loss of at least 1.7% will make the LASER fail.

## 6.2 Higher Order Modes

Higher order transverse modes have nodes. As such, they can be selected by placing a thin wire in the bath of the beam in this node. It will block enough light to stop lasing in modes without a node at that point. Leaving the lowest order mode with a node at that point lasing. Experimentally we did this by placing cross-hairs in the beam. They were adjusted until modes were visible. Modes are labelled by their number of nodes in x and y direction e.g. (0,0) for a Gaussian beam. These were imaged and can be seen in Figure 6.3. The argument could be made that the wire was simply casting a shadow, this can clearly be shown to be false in any mode with two nodes, as there was only one wire. Higher order modes than the ones shown could not be found. This is likely due to the diminishing brightness at higher orders that made (2,1), and (1,2) hard to achieve. Further, higher orders have smaller structures so a thinner, more precise wire would be needed to select them.

A comparison with known results such as those in [4] would suggest that our modes (l,m) refer to the TEM<sub>l,m</sub> states in literature.

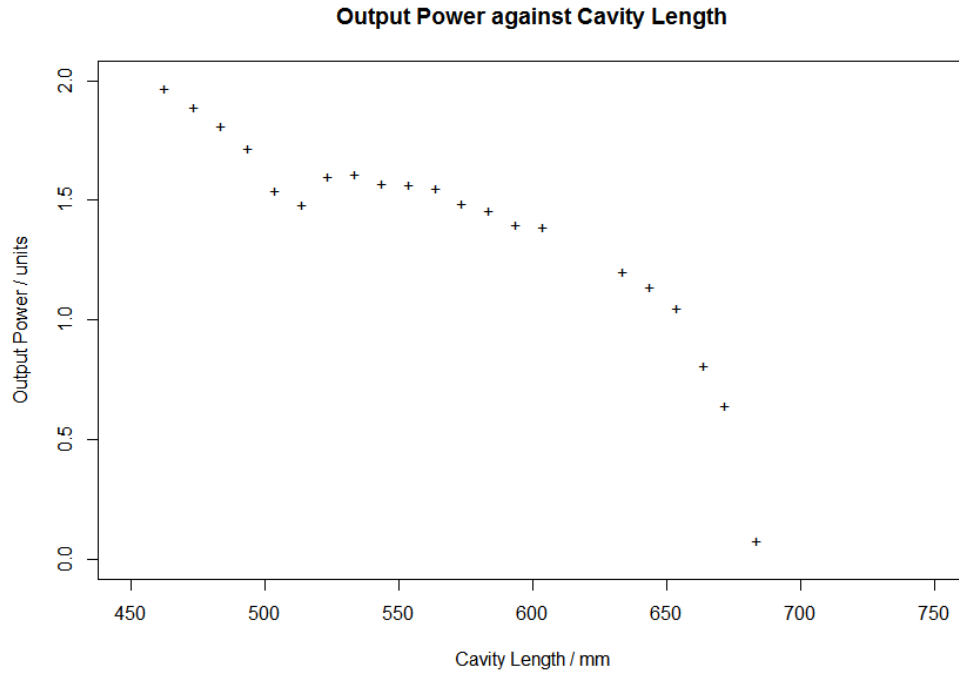


Figure 6.1: Output power of helium-neon LASER measured by photodiode in normalised arbitrary units at 632.8nm plotted against optical cavity length. Tabulated data is available in Table C.2

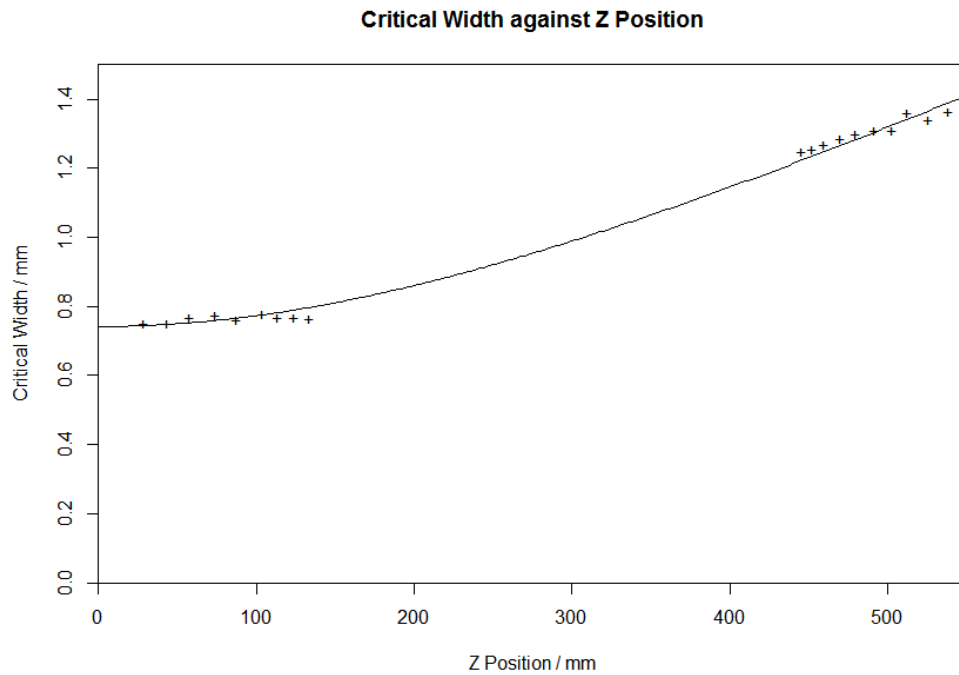
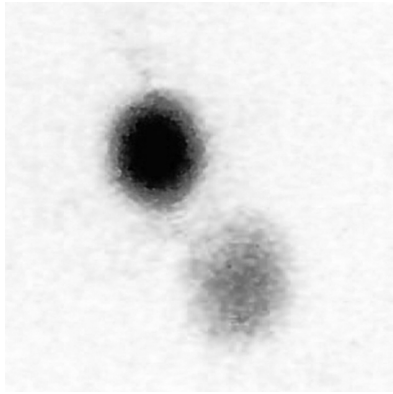


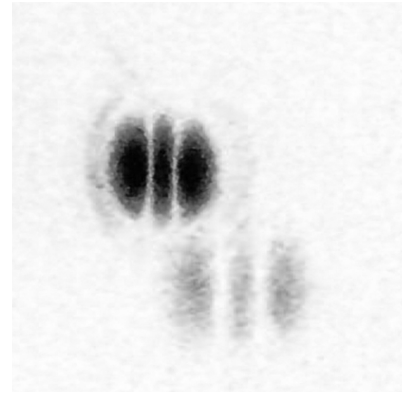
Figure 6.2: Critical width of rectangular slit to cease operation of helium-neon LASER plotted against slit position within optical cavity. Note that the gap in data collection is due to the position of the discharge tube. The solid line is a fit against Equation (6.2). Tabulated data is available in Table C.3



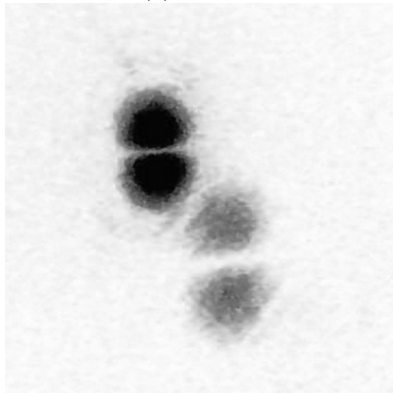
(a) TEM<sub>00</sub>



(b) TEM<sub>10</sub>



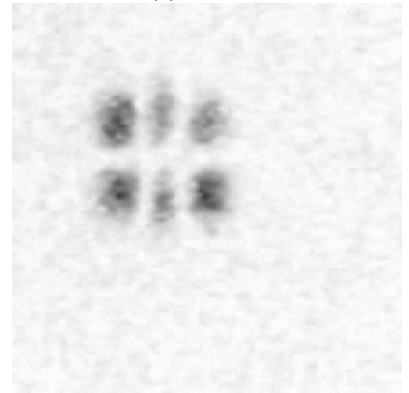
(c) TEM<sub>20</sub>



(d) TEM<sub>01</sub>



(e) TEM<sub>11</sub>



(f) TEM<sub>21</sub>



(g) TEM<sub>02</sub>



(h) TEM<sub>12</sub>

Figure 6.3: All Visible Transverse Modes

## 7 Conclusions

Throughout this experiment we built an open cavity He-Ne LASER and investigated methods of mode and frequency selection. The benefits of SLM Operation were inspected but further research would be needed to gather useful data. A number of further experiments could be carried out in the future to further this research.

The various available wavelengths near the 632.8nm line could be easily found and measured by using any number of spectroscopy techniques. A more precise frequency selector such as an etalon could be driven and the power and frequency of the output beam measured and plotted against each other. Or more simply, the LASER could be run without any mode selection and the output could be analysed with already sophisticated spectroscopy equipment such as a grating spectrometer.

While the final part of our experiment could not be completed, it is clear how to update the set-up to achieve results. With higher grade optical instruments the beam could have been expanded for interferometry experiments without introducing patterns or significant dispersion. This would allow coherence lengths to be measured directly.

Temporal interference (beating) between different frequencies could also be looked at using a fast photodiode and oscilloscope. This could allow continuous wave LASERs to be compared to modelocked pulsed LASERs.

## A Transmission of Gaussian Beam through a vertical slit

$$\begin{aligned}
 T &= \frac{\int_{-\infty}^{\infty} dy \int_{-w_s/2}^{w_s/2} dx I(z, r)}{\int_{-\infty}^{\infty} dy \int_{-\infty}^{\infty} dx I(z, r)} \\
 &= \frac{\int_{-w_s/2}^{w_s/2} \exp\left\{-2\left[\frac{x}{w(z)}\right]^2\right\} dx}{\int_{-\infty}^{\infty} \exp\left\{-2\left[\frac{x}{w(z)}\right]^2\right\} dx} \\
 &= \frac{\int_{-w'_s/2}^{w'_s/2} \exp\{-2x'^2\} dx'}{\int_{-\infty}^{\infty} \exp\{-2x'^2\} dx'}
 \end{aligned} \tag{A.1}$$

Clearly  $T$  is just a function of  $w'_s$ . So our critical transmission, at which lasing just stops occurs at a constant:

$$w'_{s,crit} = \frac{w_{s,crit}(z)}{w(z)} \tag{A.2}$$

$$\therefore w_{s,crit}(z) \propto w(z) \tag{A.3}$$

## B Demonstrating our etalon allows for SLM Operation

We require the HWHM of the etalon transmission to be less than Longitudinal Mode spacing. And that the FSR of the etalon is large enough that there won't be further peaks in the gain window.

$$\begin{aligned}
 \frac{1}{2}\delta v_{\text{FWHM}} &< \Delta v_c \\
 \Delta v_{\text{FSR}} &> \frac{1}{2}\Delta v_{osc} \\
 \mathcal{F} &\equiv \frac{\Delta v_{\text{FSR}}}{\delta v_{\text{FWHM}}}
 \end{aligned}$$

From Equation (5.1)

$$\frac{c}{2L_c} > \frac{\Delta v_{\text{FSR}}}{2\mathcal{F}}$$

Condition for SLM Operation with an Etalon with Finesse  $\mathcal{F}$ :

$$\implies L_c < 2\mathcal{F} \frac{c}{\Delta v_{osc}} \tag{B.1}$$

## C Tabulated Data

Input Current /mA	Output Power /Units		
	Test 1	Test 2	Test 3
5.00	5.55	5.53	5.56
5.10	5.68	5.68	5.70
5.20	5.80	5.80	5.81
5.30	5.92	5.91	5.94
5.40	6.02	6.01	6.02
5.50	6.11	6.12	6.15
5.60	6.20	6.20	6.24
5.70	6.28	6.30	6.32
5.80	6.34	6.39	6.40
5.90	6.41	6.45	6.46
6.00	6.49	6.52	6.53
6.10	6.54	6.57	6.59
6.20	6.60	6.62	6.65
6.30	6.64	6.67	6.70
6.40	6.67	6.71	6.75
6.50	6.70	6.75	6.78

Table C.1: Output power of helium-neon LASER measured by photodiode in normalised arbitrary units at 632.8nm plotted against input current to the discharge tube

Cavity Length /mm	Output Power /units
549	1.97
560	1.89
570	1.81
580	8.59
590	7.70
600	7.42
610	8.01
620	8.04
630	7.85
640	7.82
650	7.75
660	7.45
670	7.30
680	7.00
690	6.95
758	3.23
730	5.70
720	6.02
740	5.25
770	3.89
750	8.10

Table C.2: Output power of helium-neon LASER measured by photodiode in normalised arbitrary units at 632.8nm measured against optical cavity length at fixed input current

Critical Slit Width /mm	Slit Position /mm
612	526
640	554
625	539
599	513
589	503
578	492
566	480
556	470
546	460
538	452
532	446
220	134
210	124
200	114
190	104
174	88
160	74
144	58
130	44
115	29

Table C.3: Critical width of rectangular slit to cease operation of helium-neon LASER measured against slit position within optical cavity

## References

- [1] Chuck Leddy. “Professor Emeritus Ali Javan”. In: (Sept. 2016). URL: <https://news.mit.edu/2016/physics-professor-emeritus-ali-javan-dies-0929> (visited on 03/23/2018).
- [2] T. H. Maiman. “Stimulated Optical Radiation in Ruby”. In: *Nature* 187 (Aug. 1960), pp. 493–494. DOI: 10.1038/187493a0.
- [3] A. A. Michelson and E. W. Morley. “On the relative motion of the Earth and the luminiferous ether”. In: *American Journal of Science* Series 3 Vol. 34.203 (1887), pp. 333–345. DOI: 10.2475/ajs.s3-34.203.333. eprint: <http://www.ajsonline.org/content/s3-34/203/333.full.pdf+html>. URL: <http://www.ajsonline.org/content/s3-34/203/333.short>.
- [4] R. Paschotta. “article on ‘modes’”. In: *Encyclopedia of Laser Physics and Technology*. 1. Wiley-VCH, Oct. 2008. ISBN: 978-3-527-40828-3.
- [5] C. Webb S. Hooker. *Laser Physics*. Oxford University Press, 2010.
- [6] E. B. Saloman and Craig J. Sansonetti. “Wavelengths, Energy Level Classifications, and Energy Levels for the Spectrum of Neutral Neon”. In: *Journal of Physical and Chemical Reference Data* 33.4 (2004), pp. 1113–1158. DOI: 10.1063/1.1797771. eprint: <https://doi.org/10.1063/1.1797771>. URL: <https://doi.org/10.1063/1.1797771>.
- [7] *the helium-neon laser*. URL: [https://www-teaching.physics.ox.ac.uk/practical\\_course/scripts/srv/local/rscripts/trunk/Optics/OP35/OP35.pdf](https://www-teaching.physics.ox.ac.uk/practical_course/scripts/srv/local/rscripts/trunk/Optics/OP35/OP35.pdf) (visited on 03/23/2018).